



**HAL**  
open science

## Investigation on the preference of the martensitic structure in off-stoichiometric Ni-Mn-In alloys by first-principle calculations

Xiaomeng Liu, Jean-Marc Raulot, Claude Esling, Xiang Zhao, Liang Zuo

► **To cite this version:**

Xiaomeng Liu, Jean-Marc Raulot, Claude Esling, Xiang Zhao, Liang Zuo. Investigation on the preference of the martensitic structure in off-stoichiometric Ni-Mn-In alloys by first-principle calculations. *Journal of Magnetism and Magnetic Materials*, 2020, 514, pp.167194. 10.1016/j.jmmm.2020.167194 . hal-03491539

**HAL Id: hal-03491539**

**<https://hal.science/hal-03491539>**

Submitted on 22 Aug 2022

**HAL** is a multi-disciplinary open access archive for the deposit and dissemination of scientific research documents, whether they are published or not. The documents may come from teaching and research institutions in France or abroad, or from public or private research centers.

L'archive ouverte pluridisciplinaire **HAL**, est destinée au dépôt et à la diffusion de documents scientifiques de niveau recherche, publiés ou non, émanant des établissements d'enseignement et de recherche français ou étrangers, des laboratoires publics ou privés.



Distributed under a Creative Commons Attribution - NonCommercial 4.0 International License

**Investigation on the preference of the martensitic structure in off-stoichiometric Ni-Mn-In alloys by first-principle calculations**

Xiaomeng Liu<sup>1,2,3</sup>, Jean-Marc Raulot<sup>2,3,\*</sup>, Claude Esling<sup>2,3</sup>, Xiang Zhao<sup>1</sup> and Liang Zuo<sup>1,\*</sup>

<sup>1</sup> Key Laboratory for Anisotropy and Texture of Materials (Ministry of Education), Northeastern University, Shenyang 110819, People's Republic of China.

<sup>2</sup> Université de Lorraine, CNRS, Arts et Métiers ParisTech, LEM3, 57000 Metz, France.

<sup>3</sup>Laboratory of Excellence on Design of Alloy Metals for low-mAss Structures (DAMAS), Université de Lorraine, 57073 Metz, France.

Corresponding author: E-mail address: jean-marc.raulot@univ-lorraine.fr; lzuo@mail.neu.edu.cn

In order to figure out the effect of excess Mn atoms on the preference of the martensite structure, the tetragonal distortion was employed in the off-stoichiometric Ni-Mn-In alloys with different Mn contents using the Extra Muffin-tin Orbital combined with the Coherent Potential Approximation (EMTO-CPA). The calculations were conducted with the optimization of the magnetic structure, where the stoichiometric Ni<sub>2</sub>MnIn alloy was served as the reference. The ground state-energy-resolved tetragonal distortion reveals that the excess Mn changes the preferred stable structure from the perfect cubic  $L2_1$  structure to the tetragonally distorted structures. The stable tetragonal structure could shift from  $c/a < 1$  to  $c/a > 1$  with the increase of the Mn concentration. Furthermore, to find out more accurate preference of the martensite structure, the formation energies were calculated using different relaxation methods. The chemical disorder method with a 4-atom cell was used for the tetragonal  $L1_0$  structure by the EMTO-CPA, and the supercell method with a 96-atom cell was applied for the orthorhombic structure by the VASP at 0 K in their ferromagnetic state. The results show that, compared with the perfect cubic  $L2_1$  structure of the stoichiometric Ni<sub>2</sub>MnIn alloy, the orthorhombic structure is preferred at lower Mn concentrations (between 29 at. % and 40 at. %), whereas the tetragonal  $L1_0$  structure is more stable at the higher Mn concentrations (above 40 at. %). Moreover, the effect of the Mn concentration on the magnetic properties was also studied. With the increase of excess Mn content, the magnetic moment increases linearly in the ferromagnetic cubic  $L2_1$  structure, whereas it varies in the two kinds of martensite. The excess Mn could lead to the coexistence of ferromagnetism and antiferromagnetism. The appearance of the antiferromagnetism could be attributed to the Ni-Mn antiferromagnetic interaction in the tetragonal martensite.

**Keywords:** Ni-Mn-In alloys; martensite structure; tetragonal distortion; tetragonal  $L1_0$  structure; orthorhombic structure; first-principle calculations.

## 1. Introduction

Based on the activation mechanisms of shape memory effect, the Heusler type Ni-Mn-based alloys could be classified into two groups: (i) Ni-Mn-Ga alloys, in which the shape change is originated from the magnetic field-induced martensite variant rearrangement [1–4]; (ii) Ni-Mn-X (X = In, Sb and Sn) alloys, in which the shape change is generated from the magnetic field-induced reverse martensitic transformation [5–7]. During the cooling process, both these alloys undergo a series of transitions, including the melt to the partially disordered  $B2$  phase transition [8], the second-order  $B2 - L2_1$  transition [9] and the first-order martensitic transition. Especially, for the Ni-Mn-In alloys, the austenite could transform into two kinds of martensite phase depending on the chemical composition, *i.e.*, (i) the modulated martensite with orthorhombic or monoclinic structure, such as  $6M$  [10],  $10M$  [11] or  $4O$  [12] structures; (ii) the non-modulated martensite with tetragonal  $L1_0$  structure [13]. These structures have been previously examined by X-ray diffraction, neutron diffraction or TEM selected area electron diffraction.

For the off-stoichiometric Ni-Mn-In alloys, the ferromagnetic austenite does not directly transform to the ferromagnetic martensite, but has to go through the antiferromagnetic martensite, which is called metamagnetic transition [14,15]. That is because the extra Mn atoms may enhance the ferromagnetism in the austenite by increasing the total magnetic moment [11,16]. This results in the antiferromagnetic exchange interactions in the martensite, which could be attributed to the different hybridization of Mn-Mn atoms [16–18] or Ni-Mn atoms [19,20]. It also leads to a composition-dependent Curie temperature variation of the martensite. The Curie temperature could decrease drastically with the increased Mn concentration [6]. Moreover, the phase stabilities of austenite and martensite could vary with the Mn composition [11], and the martensitic transition temperatures would increase significantly with the additional Mn content [6,21]. Therefore, the effect of the Mn concentration on the phase stability and the magnetic properties of the austenite

and the martensite [21–23] is critical for understanding the martensitic transformation. In the previous report [16], the possibility of martensitic phase transition was studied in Ni-Mn-In alloys, where the structural transformation was realized by the tetragonal distortion and the antiferromagnetic interaction was caused by the Mn-Mn hybridization. The results showed a transition from the cubic structure into the tetragonal structure with  $c$  larger than  $a$  (in the cubic coordination system) [16]. However, the possibility of martensitic transition from the cubic structure to the tetragonal structure with  $c$  smaller than  $a$  (in the cubic coordinate system) by tetragonal distortion was not much studied. It is considered that this kind of tetragonal structure could be the origin of the orthorhombic or the monoclinic modulated structure leading to the formation of the modulated structures [6,22]. Moreover, as demonstrated by experimental observations and theoretical calculations, the antiferromagnetic interaction could also be attributed to the Ni-Mn hybridization with additional Mn content [19,20,24].

In the present work, the effect of the Mn concentration on the preference of the martensitic structure in the off-stoichiometric Ni-Mn-In alloys was studied by the tetragonal distortion using the Extra Muffin-tin Orbital method combined with the Coherent Potential Approximation (EMTO-CPA) under magnetic structure optimization. Based on the martensitic structure preference results, the phase stability of the tetragonal  $L1_0$  and the orthorhombic structures in the ferromagnetic state were calculated by chemical disorder method within the EMTO-CPA and the supercell method within the VASP. The formation energies were compared with the cubic  $L2_1$  structure of the off-stoichiometric Ni-Mn-In alloys with different Mn contents. Furthermore, the effect of the Mn concentration on the total magnetic moment was calculated for the three structures in the ferromagnetic state. The type of antiferromagnetic interaction within the tetragonal  $L1_0$  martensite in the ferromagnetic and antiferromagnetic coexisting state was also analyzed.

## **2. Computational method**

Before constructing the crystal structures of the off-stoichiometric Ni-Mn-In alloys, the preferred site of the excess Mn atoms with an amount of 6.25 at. % in a unit cell with 16 atoms was determined by the formation energies using the Vienna Ab-initio Simulation Package (VASP) [25]. The conventional cell of the cubic  $L2_1$  Ni<sub>2</sub>MnIn alloy is presented in Fig. 1. In the figure, the primitive cell is also outlined with the dashed lines. Here, the atomic combination of the primitive cell (4 atoms) is defined as a motif, and it is used as one of the structure units for calculating the formation energy and total magnetic moment of other structures (tetragonal and orthorhombic, as described later). The full charge density method was applied to treat the tetragonal distortion by the Extra Muffin-Tin Orbital method combined with the Coherent Potential Approximation (EMTO-CPA) [26–28] with the optimization of the magnetic structure. For the phase stability analysis of the tetragonal  $L1_0$  martensite of the Ni-Mn-In alloys with different Mn concentrations, the more efficient EMTO-CPA was used. For the simulation of the orthorhombic martensite structures with different Mn concentrations, a cell containing 96 atoms was constructed with the supercell method allowing volume relaxation using the VASP. The Generalized Gradient Approximation (GGA), established by Perdew, Burke, and Ernzerhof (GGA-PBE) [29], was employed to describe the exchange-correlation functions. The electronic configurations were Ni ( $3d^84s^2$ ), Mn ( $3d^64s^1$ ), and In ( $4s^24p^1$ ), respectively. Based on the convergence test, the reciprocal-grid density of  $12 \times 12 \times 12$  Gamma centered Monkhorst-Pack k-point meshes for the  $L2_1$  primitive cell and 420 eV as the kinetic energy cutoff were applied in the VASP calculations. The EMTO was performed with a basis set including the  $s, p, d, f$  orbitals. After carefully testing the convergence of the equilibrium parameter against the k-point meshes, a  $13 \times 13 \times 13$  k-point meshes was set for the primitive cell with 4 atoms. The formation energy ( $E_f$ ) of the Ni<sub>2</sub>Mn<sub>x</sub>In<sub>2-x</sub> was determined according to the following function of the Mn concentration ( $x$ ):

$$E_f(x) = E_0(\text{Ni}_2\text{Mn}_x\text{In}_{2-x}) - 2 * E_{\text{Ni}} - x * E_{\text{Mn}} - (2 - x) * E_{\text{In}}$$

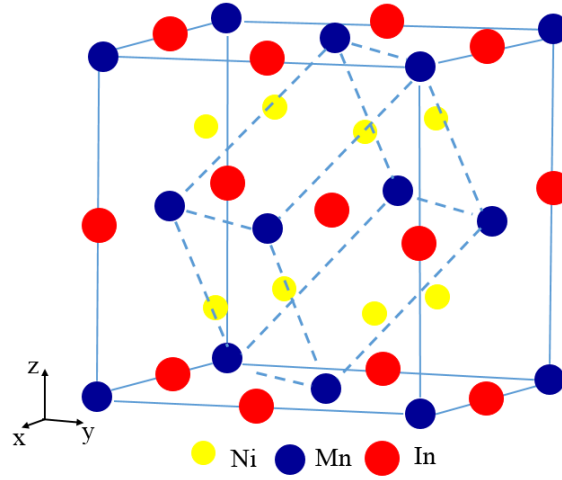


Fig. 1 Crystal structure of cubic  $L2_1$   $\text{Ni}_2\text{MnIn}$  austenite. The solid lines outline a conventional cell with 16 atoms and the dashed lines outline a primitive cell with 4 atoms.

### 3. Results and discussion

#### 3.1 Preferred site of excess Mn

To find out the sublattice site preference of the excess Mn atoms, the formation energies of different point defects within the 16-atom cell (Fig. 1) were tested by crystal structure optimization using VASP. The calculated formation energies of the perfect austenite and the austenite with 6.25 at. % point defects are shown in Table 1. It is seen that the values of the point defect formation can be positive or negative, but all the formation energies of the defected structures are larger than those of the perfect austenite. This indicates that the point defect will reduce the ground state stability of the ferromagnetic cubic structures. Among all the defected structures, the sublattice with the substitution of Mn for In ( $_{\text{In}}\text{Mn}$ ) possesses the lowest negative defect formation energy, which infers that this kind of point defect could exist steadily. Therefore, the excess Mn substituting for In was employed for the further study of the influence of Mn content on the martensitic structure preference in the off-stoichiometric Ni-Mn-In alloy. Note that the antisite defect with Mn substituting for Ni is not converged at 0 K, which indicates that the cubic structure of  $\text{Ni}_{50}$ -

$x\text{Mn}_{25+x}\text{In}_{25}$  alloy could not exist at 0 K. This discovery is consistent with the fact that there is no evidence of such kinds of alloys in the previous experimental investigations.

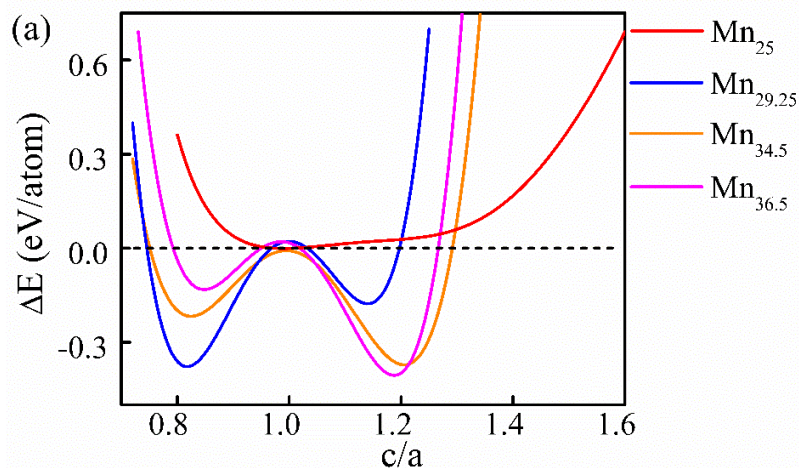
Table 1 Optimized lattice parameters and formation energy of perfect austenite and austenite with point defect for a 16-atom cell (v\_element indicates vacancy situation)

	$a/(\text{\AA})$	$E_f/(\text{eV/unit cell})$		$a/(\text{\AA})$	$E_f/(\text{eV/unit cell})$
v_Ni	6.0261	-0.584	inMn	6.0645	-0.850
v_In	5.9195	0.522	Ni <sub>8</sub> Mn <sub>4</sub> In <sub>4</sub>	6.0607	-1.130

### 3.2 Tetragonal distortion

As the stable structure of the Ni-Mn-X alloys could be changed with the type and the concentration of the element X [13], the tetragonal and the orthorhombic distortions can be applied to simulate the martensitic phase transition [30]. The non-modulated martensite with a tetragonal  $L1_0$  structure is related to a distorted cubic structure with  $c$  larger than  $a$ . The modulated martensite with a monoclinic structure, like the orthorhombic structure, is originated from a distorted cubic structure with  $c$  less than  $a$ , as reported in the literature [11]. Moreover, the previous experimental observation revealed that the martensite exhibits a coexistence of ferromagnetic and antiferromagnetic interactions in the off-stoichiometric alloys. The antiferromagnetic interaction could be originated from Mn-Mn [16–18] or Ni-Mn hybridization [19,20]. It has been shown that the martensitic transition could not happen from the cubic  $L2_1$  austenite to the tetragonal  $L1_0$  martensite in the stoichiometric alloy [16]. Nevertheless, for the compounds with Mn concentrations ranging from 32.5 at. % to 40 at. %, the transformation could happen from the ferromagnetic cubic  $L2_1$  austenite to the co-existing ferromagnetic and antiferromagnetic tetragonal  $L1_0$  martensite. The antiferromagnetic interaction is supposed to come from the Mn-Mn hybridization by tetragonal distortion. However, the martensitic transformation from the cubic

austenite to the modulated monoclinic martensite remains unclear. In order to figure out the effect of the Mn concentration on the martensite structure preference of the off-stoichiometric  $\text{Ni}_{50}\text{Mn}_x\text{In}_{50-x}$  alloys and to reveal the antiferromagnetic interaction between the atoms, the tetragonal distortion was applied to determine the possible stable structures at 0 K for the first step. For the calculations, the  $c/a$  value is limited between 0.7~1.6, and no structural relaxation was conducted. The energies of different structures were calculated using the efficient EMTO-CPA method with the optimization of the magnetic structure. The calculated results were represented with the ground state energy difference between the distorted structure and the initial cubic structure at every Mn concentration. Based on the point defect formation energy analysis, four  $\text{Ni}_{50}\text{Mn}_x\text{In}_{50-x}$  alloys ( $x = 25, 29.25, 34.5$  and  $36.5$ ) with the excess Mn substituting for In ( $\text{InMn}$ ) were used. First, we set the ground state energy of the cubic structure ( $c/a = 1$ ) of each alloy to be the reference state, *i.e.*, 0 eV. Then, the ground state energy difference between the distorted structure and its reference state was calculated as a function of the  $c/a$  ratio for each alloy, and the results are shown in Fig. 2 (a). It should be mentioned that the small deviations from 0 eV at  $c/a = 1$  for the alloys with 29.25 at. % and 36.5 at. % Mn were caused by the curve fitting.



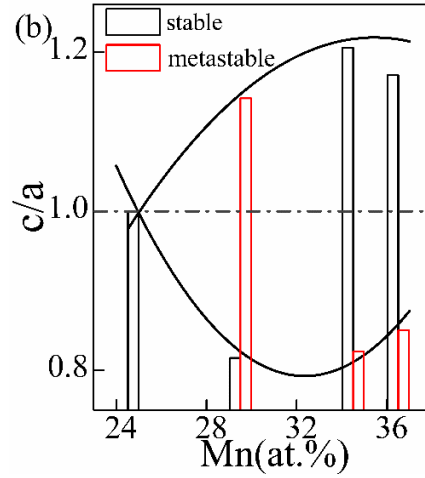


Fig. 2 (a) Variation of ground state energy difference as a function of tetragonal distortion ( $c/a$  ratio) in Ni-Mn-In alloys with different Mn contents. (b)  $c/a$  ratio value of local minimum energy point of Ni-Mn-In alloys with different Mn contents. Parabola curves indicate  $c/a$  ratio value of local minimum energy point for  $c/a < 1$  and  $c/a > 1$ .

It is seen from Fig. 2 (a) that, for the stoichiometric  $\text{Ni}_{50}\text{Mn}_{25}\text{In}_{25}$  compound, the perfect cubic structure with  $c/a = 1$  possesses the minimum ground state energy. This reveals that the cubic structure is the most stable state and is hard to undergo any martensitic transformation, which corresponds to the previous calculation result [31]. In contrast, the ground state energy difference between the tetragonally distorted structure and the cubic structure of the off-stoichiometric  $\text{Ni}_{50}\text{Mn}_x\text{In}_{50-x}$  alloys is negative for both  $c/a > 1$  and  $c/a < 1$  distortions. The  $\text{Ni}_{50}\text{Mn}_{29.25}\text{In}_{20.75}$  alloy has the lowest local minimum energy in the  $c/a < 1$  case, whereas the  $\text{Ni}_{50}\text{Mn}_{36.5}\text{In}_{13.5}$  alloy has the lowest local minimum energy in the  $c/a > 1$  case. Since the structure having local minimum ground state energy difference corresponds to the possible stabilized tetragonal structure, we could deduce that the tetragonal structure becomes preferred than the cubic  $L2_1$  structure with the excess Mn, and the different Mn content results in different types of tetragonal structure. These results are in good agreement with the experimental results which evidenced that the excess Mn content enhances the stability of the martensite [11]. Moreover, for each off-stoichiometric concentration, there exist two local minima, with the one being higher than the other, as shown in Fig. 2 (a). The

structure corresponding to the lower minimum should be the stable structure, whereas that to the higher minimum should be the metastable structure. Taking the concentration of 29.25 at. % Mn as an example, one can find that the stable structure is the one with  $c/a = 0.81$ , and the metastable structure is the one with  $c/a = 1.14$ . Furthermore, to find out the relationship between the possible preferred stable structure and the excess Mn contents, the tetragonal distortion with  $c/a > 1$  and  $c/a < 1$  possessing local minimum energy at different Mn concentrations were fitted, and the curves are displayed in Fig. 2 (b). In general, the curves of the relative ground state energy as a function of the  $c/a$  ratio show a parabolic shape for both  $c/a < 1$  and  $c/a > 1$  distortions in the off-stoichiometric Ni-Mn-In alloys. For the tetragonal distortion with  $c/a > 1$ , the  $c/a$  value corresponding to the local minimum energy increases with the increased Mn content first and then decreases. However, for the tetragonal distortion with  $c/a < 1$ , the tendency is opposite. The  $c/a$  value corresponding to the local minimum energy decreases first and then increases when the Mn concentration is larger than 34.5 at. %. As the tetragonal distortion  $c/a$  value of the stable and metastable structure varies with Mn concentration, for clarity, the stable and metastable state corresponding to the two types of local minimum energy were highlighted with the histograms at each composition in Fig. 2 (b). It is seen that the stable structure shifts from the tetragonal structure with  $c/a < 1$  to  $c/a > 1$  with the increasing Mn concentration, whereas the metastable structure changes from the tetragonal structure with  $c/a > 1$  to  $c/a < 1$ . The stable structure with tetragonal distortion  $c/a < 1$  only appears in the alloy with 29.25 at. % Mn. When the Mn concentration further increases to 34.5 at. % and above, the stable structures are those with tetragonal distortion  $c/a > 1$ . Therefore, we could deduce that the tetragonal structure stability would be enhanced with the extra Mn added, and the preferred martensitic structure changes from the tetragonal structure with  $c/a < 1$  to that with  $c/a > 1$ . This result agrees with the observation that the alloys with lower Mn

concentration showed the tetragonality related to the modulated structures [13], and the alloys with higher Mn concentration showed the tetragonal  $L1_0$  structure [11].

### 3.3 Phase stability

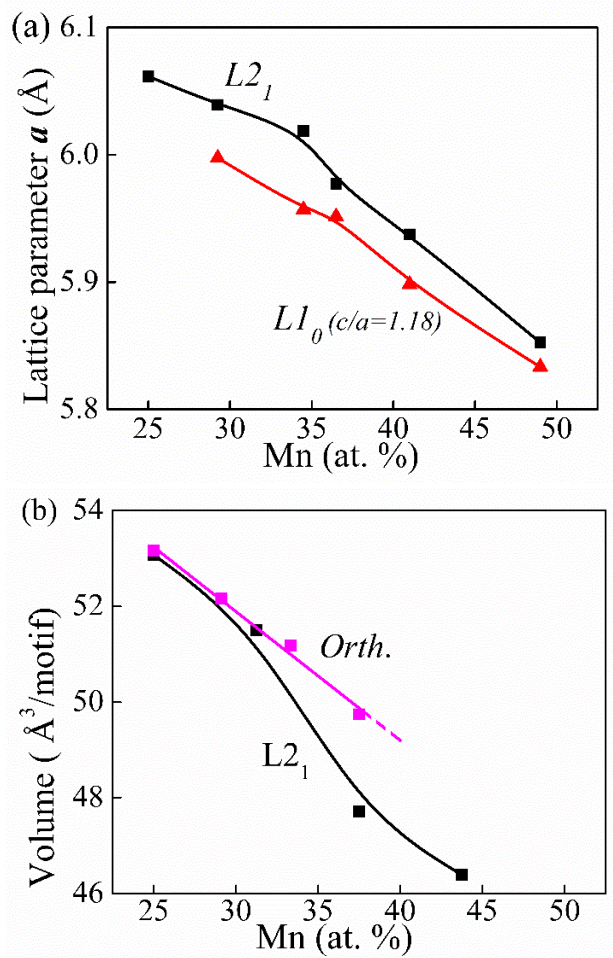


Fig.3 (a) Optimized lattice parameter ( $a$ ) of ferromagnetic cubic  $L2_1$  and tetragonal  $L1_0$  ( $c/a = 1.18$ ) structures; (b) optimized cell volume of ferromagnetic cubic  $L2_1$  and orthorhombic structures (Dashed-line indicates extrapolation of the fitting.)

Based on the above results of tetragonal distortion, the preference of the martensitic transition to the different tetragonal structures was analyzed for the off-stoichiometric Ni-Mn-In alloys with the extra Mn added. As the accurate structure of the preferred martensitic structure under the effect of the Mn concentration is still not clear, we constructed the tetragonal  $L1_0$  structure (space group:  $I4/mmm$ , [32]) and the orthorhombic structure (originated from the monoclinic  $6M$  martensite [10])

which correspond to the respective tetragonal structure with  $c/a > 1$  and  $c/a < 1$  in the tetragonal distortion. The formation energies of the two structures with different Mn concentrations were calculated in the ferromagnetic state, and further compared with that of the perfect cubic  $L2_1$  structure. Since the previous experimental observation found that the Curie temperature of the tetragonal martensite ranges from 200 K to 50 K [11,13], we only considered the ferromagnetic state for the martensite with the tetragonal  $L1_0$  and the orthorhombic structures in this step. In the present work, firstly, we did the optimization test for the  $c/a$  values of the tetragonal  $L1_0$  structure with a series of lattice parameter ( $a$ ) using the tetragonal distortion under the Equation of State with the Morse function for the  $\text{Ni}_{50}\text{Mn}_{29.25}\text{In}_{20.75}$  and  $\text{Ni}_{50}\text{Mn}_{34.5}\text{In}_{15.5}$  alloys by the EMTO-CPA. We found that the  $c/a$  ratio showed little dependence on the Mn concentration. For the  $c/a$  ratio value around  $c/a = 1.18$ , the variation is within 0.05. Therefore, we adopt the  $c/a = 1.18$  for the tetragonal  $L1_0$  structure at all the concentrations for the optimization of their lattice parameter  $a$ . The optimized lattice parameter ( $a$ ) of the cubic  $L2_1$  and the tetragonal  $L1_0$  structures in the ferromagnetic ground state is shown in Fig. 3 (a). It is seen that the lattice parameters of the two structures show a composition dependence for all the alloys. For the ferromagnetic  $L2_1$  structure, the optimized lattice parameter decreases regularly with the increase of the extra Mn. This is consistent with the actual lattice parameter of the ferromagnetic austenite in the stoichiometric alloy ( $a = 6.072 \text{ \AA}$ ) [16] and in the off-stoichiometric alloy ( $a = 6.016 \text{ \AA}$ ) [15]. The lattice parameter ( $a$ ) of the tetragonal  $L1_0$  structure shows the same tendency which could be attributed to the smaller atomic radius of the Mn atom. The martensite with an orthorhombic structure was also calculated with volume relaxation for the  $\text{Ni}_{50}\text{Mn}_x\text{In}_{50-x}$  alloys. Since the EMTO-CPA is too complicated to relax the three lattice parameters, the alloys with different Mn contents were constructed with the supercell method in the VASP with the relaxation of the cell volume and the atom positions. The optimized volume of the cubic  $L2_1$  and the orthorhombic (*Orth.*) structures were obtained, and the

results are displayed in Fig. 3 (b). We truncated the Mn concentration at 37.5 at. % for the orthorhombic structure since the  $6M$  structure was measured in the Ni-Mn-In alloys with 36 at. % Mn [10]. The volumes of the two structures decrease with the extra Mn added. The volume of the  $L2_1$  structure shows an abrupt decrease after 29 at. % and becomes smaller than that of the orthorhombic structure. In contrast, the volume of the orthorhombic structure decreases linearly with the increase of the Mn concentration. Such a volume change tendency is opposite to the experimental observation which demonstrated that the martensite transition from  $L2_1$  to the  $6M$  structure was a volume compression process [33]. This discrepancy may be caused by the original orthorhombic structure setting, as the cell shape was fixed during the calculations.

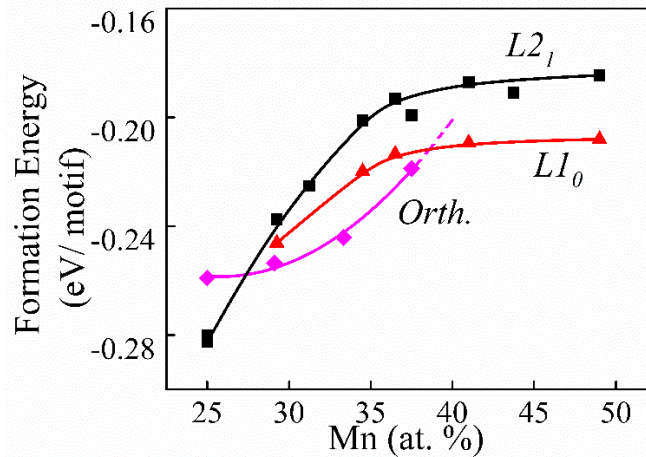


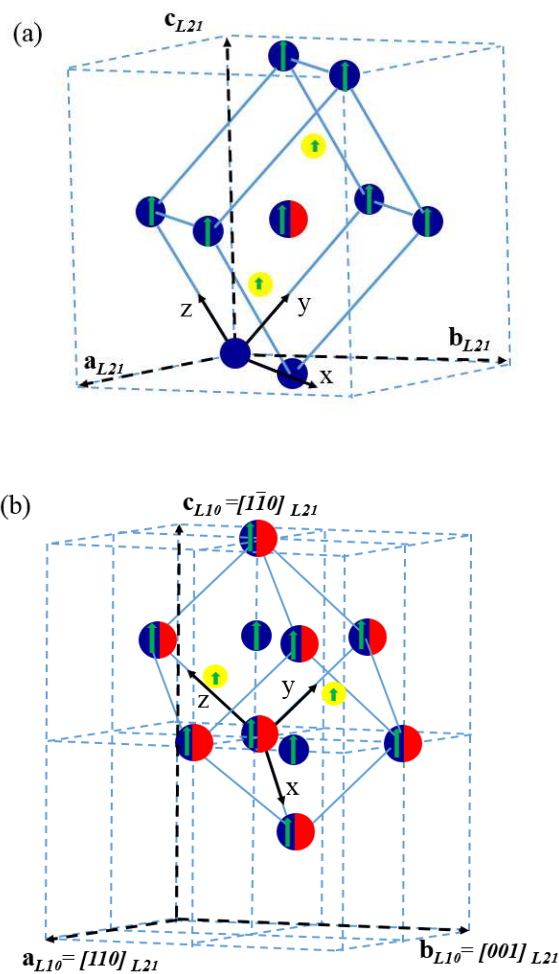
Fig.4 Formation energy of ferromagnetic cubic  $L2_1$ , tetragonal  $LI_0$  with  $c/a = 1.18$  and orthorhombic structures as a function of Mn concentration (Dashed-line indicates extrapolation of the fitting.)

Based on the obtained equilibrium lattice parameters, the formation energies of the cubic  $L2_1$ , the tetragonal  $LI_0$  ( $c/a = 1.18$ ) and the orthorhombic structures were calculated to analyze the preference of the martensitic structure, as shown in Fig. 4. For the stoichiometric  $Ni_2MnIn$  alloy, the cubic  $L2_1$  structure still possesses the lowest formation energy. This result further confirms that the stoichiometric cubic structure is the stable structure at 0 K, which agrees with the above tetragonal distortion results (Fig. 2 (b)). With the excess Mn added, the formation energies of the

three structures increase with the Mn content. This indicates that the stability of all the three structures of the off-stoichiometric Ni-Mn-In alloys with the extra Mn would be lowered. The tetragonal  $L1_0$  and the orthorhombic structures show lower formation energy than the cubic  $L2_1$  structure at the compositions higher than 29 at. % Mn, indicating that the two kinds of martensite are more stable than the cubic austenite with the excess Mn added in the off-stoichiometric Ni-Mn-In alloys in the ferromagnetic state. Comparing the formation energy of the cubic  $L2_1$  with that of the orthorhombic structure, one can find that the difference increases first and then decreases with the largest formation energy difference appearing at about 33 at. % Mn (Fig. 4). However, the formation energy difference between the cubic  $L2_1$  and the tetragonal  $L1_0$  structures increases first and then keeps roughly constant at compositions higher than 40 at. % Mn (Fig. 4). If we compare the formation energies between the two kinds of martensite, we can also find that the orthorhombic structure with about 29 at. % Mn is lower, meaning that the orthorhombic martensite is more stable. This is consistent with the result of the tetragonal distortion test during which the most stable tetragonal structure with  $c/a < 1$  appears in the alloy having 29.25 at. % Mn (Fig. 2 (b)). However, according to the variation tendency of the formation energies of the two kinds of martensite, the formation energy of the tetragonal  $L1_0$  structure becomes smaller than that of the orthorhombic structure at about 40 at. %. This is different from the result predicted by the above tetragonal distortion analysis (Fig. 2 (b)). In that prediction, the smallest Mn content when the tetragonal  $L1_0$  structure becomes stable is about 34.5 at. % (Fig. 2 (b)). The discrepancy may be caused by the different first principle methods for the tetragonal distortion in the tetragonal  $L1_0$  and the orthorhombic structure calculations, each having a different relaxation limitation. Despite the discrepancy, this result indicates that the orthorhombic structure is preferred between 29 at. % and 40 at. % Mn, and the tetragonal  $L1_0$  structure becomes more stable at the compositions above 40 at. % Mn. Thus, the orthorhombic structure is preferred at lower Mn concentrations, and the

tetragonal  $L1_0$  structure becomes favored at higher Mn concentrations. This result agrees with the previous report that the ground state structure of the  $\text{Ni}_{50}\text{Mn}_x\text{In}_{50-x}$  (with  $29 \leq x \leq 40$ ) alloy is the modulated martensite with the monoclinic structure, and the ground state structure of the  $\text{Ni}_{50}\text{Mn}_x\text{In}_{50-x}$  (with  $40 \leq x \leq 50$ ) alloy is the non-modulated martensite with the tetragonal  $L1_0$  structure [11,34]. Thus, we could deduce that the excess Mn would enhance the possibility of the martensitic transition from the austenite with the cubic structure to the martensite with the orthorhombic or the tetragonal structure. The preferred martensitic structure between the orthorhombic and the tetragonal  $L1_0$  structure is determined by the Mn concentration.

### 3.4 Magnetic property



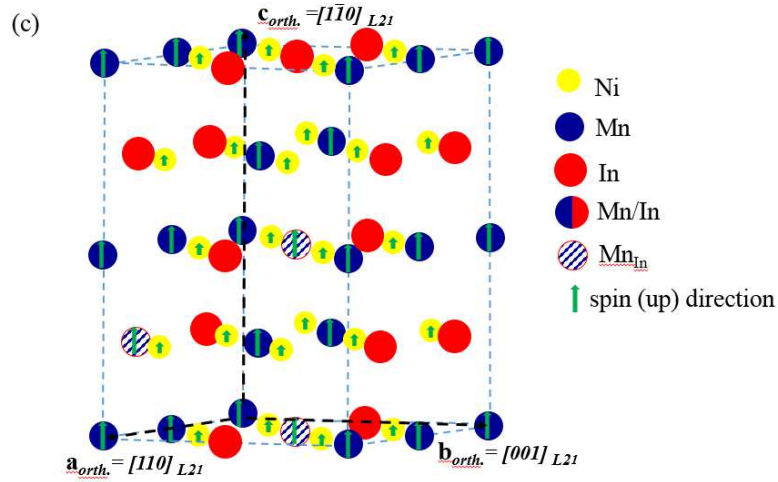


Fig. 5 (a) Primitive cell of cubic  $L2_1$  structure, (b) primitive cell of tetragonal  $L1_0$  structure and (c) conventional cell of orthorhombic structure of ferromagnetic off-stoichiometric Ni-Mn-In alloy (34.375 at. % Mn) with excess Mn substituting for In. The spin-up directions of atomic sites are indicated. (Mn/In indicates the excess Mn and In at the same site. Mn<sub>In</sub> indicates the excess Mn substituting for In.)

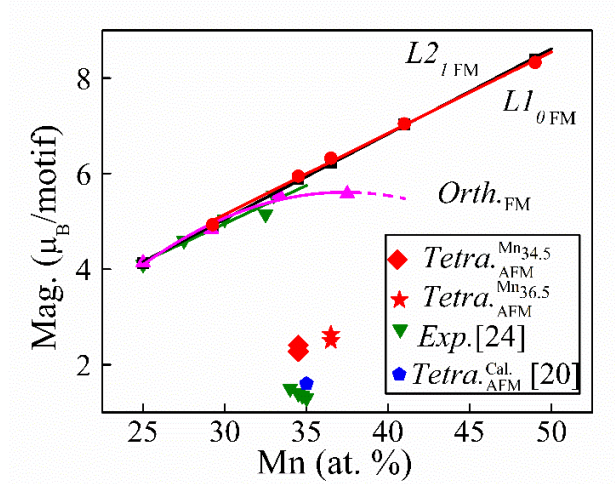


Fig. 6 Total magnetic moment of cubic  $L2_1$ , tetragonal  $L1_0$  and orthorhombic structure in off-stoichiometric Ni-Mn-In alloys with different Mn contents in the ferromagnetic state and tetragonal structures of  $Ni_{50}Mn_{34.5}In_{15.5}$  and  $Ni_{50}Mn_{36.5}In_{13.5}$  alloys at ferromagnetic and antiferromagnetic coexisting state. (Dashed-line indicates extrapolation of the fitting.)

Furthermore, with the aim to figure out the effect of the Mn concentration on the magnetic properties of the three structures, the total magnetic moment of one motif of the three structures was also calculated for the off-stoichiometric alloys with different Mn contents in the

ferromagnetic state. As an example, the unit cells of the alloy with 34.375 at. % Mn are illustrated in Fig. 5, where the spin (up) direction of each atomic site is indicated. In the figure, the  $L2_1$  and  $L1_0$  structures were constructed by the Coherent Potential approximation [35] (Fig. 5 (a) and (b)). However, the orthorhombic structure was constructed by the supercell approach [36] (Fig. 5 (c)), and here we show it conventional cell with 32 atoms. The calculated magnetic moment results are displayed in Fig. 6. It is seen that the total magnetic moment of the cubic  $L2_1$  and that of the tetragonal  $L1_0$  structure show an increase with the excess Mn concentration for all the compositions, and the magnetic moment difference between the martensite and the austenite is quite small. For the ferromagnetic orthorhombic structure, the total magnetic moment shows a parabolic tendency which increases with the Mn content first and then tends to decrease after the 37.5 at. % Mn content. We could find that the total magnetic moment of the alloys with Mn content less than 34 at. % increases with the Mn content, which agrees with the experimental measurements [22]. There is no decrease in the total magnetic moment of all the structures with different Mn content in the ferromagnetic state in the present work. However, in Ref. [22], the total magnetic moment was found to decrease abruptly above 34 at. % Mn.

Then, we carried out the calculation on the total magnetic moment of the 34.5 at. % and the 36.5 at. % Mn alloy with the tetragonal structure. These two compounds possess the local minimum energy in the tetragonal distortion (*i.e.*, the tetragonal structure with  $c/a < 1$  corresponds to the orthorhombic martensite, and  $c/a > 1$  corresponds to the tetragonal  $L1_0$  martensite). During the calculation, the magnetic structure was optimized. Compared with the ferromagnetic martensite, the total magnetic moment of the martensite with tetragonal structures for these two alloys shows an abrupt decrease to around  $2.5 \mu_B$ . The magnetic moment of the Ni atoms shows antiferromagnetism with a value of about  $-0.2\mu_B$  and that of Mn shows ferromagnetism with a

value decreasing to  $2.25 \mu_B$ . The results suggest the coexistence of the ferromagnetism and antiferromagnetism in these two concentrations. The antiferromagnetic interaction could be originated from the Ni-Mn hybridization interaction, which is consistent with the theoretical calculation result of the tetragonal structure [19], as displayed in Fig. 6. Considering that the Mn content (around 34 at. %) is certificated as the phase transformation point from the cubic to the martensitic structure [11,17], the total magnetic moment of the tetragonal structures with 34.5 at. % and 36.5 at. % Mn were in good agreement with the experimental observation at 5 K [22]. Therefore, we could assert that the excess Mn could linearly enhance the ferromagnetism of the austenite, whereas the excess Mn results in a more complex magnetic state in the martensite. The higher Mn concentration could give rise to a coexistence of the ferromagnetism and the antiferromagnetism in the two martensite structures. The antiferromagnetic interaction could be attributed to the Ni-Mn hybridization.

#### 4. Summary

In the present work, we analyzed the effect of Mn concentration on the preference of martensitic phase transition in off-stoichiometric Ni-Mn-In alloys. The structural stability of cubic  $L2_1$  austenite, tetragonal  $L1_0$ , and orthorhombic martensite were evaluated by the first-principle calculations. The formation energies of point defect types (vacancy and antisite) around stoichiometric  $Ni_2MnIn$  alloys in the ferromagnetic state were calculated systematically, and the preference substitution of the excess Mn atoms was then determined. Based on the Mn substitution preference, the tetragonal distortion was calculated for the off-stoichiometric Ni-Mn-In alloys with different Mn concentrations by the EMTO-CPA with magnetic structure optimization. The results showed that the tetragonal structure stability could be enhanced with the additional Mn, and the cubic  $L2_1$  structure becomes less stable. With the increasing Mn concentration, the preferred stable tetragonal structure evolves from the tetragonal structure with  $c/a < 1$  to the one with  $c/a > 1$ . In

order to find out the accurate phase stability of the off-stoichiometric Ni-Mn-In alloys with tetragonal structures for both  $c/a < 1$  and  $c/a > 1$  at 0 K, the formation energies of the tetragonal  $L1_0$  and orthorhombic structures were calculated with structure optimization in the ferromagnetic state, respectively. As compared with the cubic  $L2_1$  structure, the orthorhombic structure is preferred at lower Mn concentrations, and the tetragonal  $L1_0$  structure becomes preferred at higher Mn concentrations. Furthermore, the total magnetic moment of the ferromagnetic cubic  $L2_1$  and tetragonal  $L1_0$  structures are strengthened with the increase of Mn content, whereas that of the orthorhombic structure shows a parabolic tendency with a decreasing tendency after 37.5 at. % Mn. Under the magnetic structure optimization, the total magnetic moment of the tetragonal structure decreases abruptly after 34.5 at. % Mn. The high Mn concentration could result in the coexistence of ferromagnetism and antiferromagnetism. The latter could be attributed to the Ni-Mn antiferromagnetic hybridization.

### **Acknowledgements**

This work was supported by the National Natural Science Foundation of China (Grant No. 51431005), the National High Technology Research and Development Program of China (Grant No. 2015AA034101), the LiaoNing Revitalization Talents Program (Grant No. XLYC1802023) and the Programme of Introducing Talents of Discipline Innovation to Universities 2.0 (No. BP0719037).

### **References**

- [1] V.A. Chernenko, V. V. Kokorin, O.M. Babii, I.K. Zasimchuk, Phase diagrams in the Ni-Mn-Ga System under compression, *Intermetallics*. 6 (1998) 29–34. doi:10.1016/S0966-9795(97)00050-2.
- [2] K. Ullakko, J.K. Huang, C. Kantner, R.C. O’Handley, V. V. Kokorin, Large magnetic-field-induced strains in  $\text{Ni}_2\text{MnGa}$  single crystals, *Appl Phys Lett*. 69 (1996) 1966–1968. doi:10.1063/1.117637.
- [3] R.C. O’Handley, Model for strain and magnetization in magnetic shape-memory alloys, *J Appl Phys*. 83 (1998) 3263–3270. doi:10.1063/1.367094.

- [4] R.D. James, M. Wuttig, Magnetostriction of martensite, *Philos Mag A*. 77 (1998) 1273–1299. doi:10.1080/01418619808214252.
- [5] R. Kainuma, Y. Imano, W. Ito, Y. Sutou, H. Morito, S. Okamoto, O. Kitakami, K. Oikawa, A. Fujita, T. Kanomata, K. Ishida, Magnetic-field-induced shape recovery by reverse phase transformation, *Nature*. 439 (2006) 957–960. doi:10.1038/nature04493.
- [6] Y. Sutou, Y. Imano, N. Koeda, T. Omori, R. Kainuma, K. Ishida, K. Oikawa, Magnetic and martensitic transformations of NiMnX (X = In, Sn, Sb) ferromagnetic shape memory alloys, *Appl. Phys. Lett.* 85 (2004) 4358–4360. doi:10.1063/1.1808879.
- [7] I. Karaman, H.E. Karaca, B. Basaran, D.C. Lagoudas, Y.I. Chumlyakov, H.J. Maier, Stress-assisted reversible magnetic field-induced phase transformation in Ni<sub>2</sub>MnGa magnetic shape memory alloys, *Scr Mater.* 55 (2006) 403–406. doi:10.1016/j.scriptamat.2006.03.061.
- [8] R. McCormack, D. de Fontaine, First-principles study of multiple order-disorder transitions in Cd<sub>2</sub>AgAu Heusler alloys, *Phys Rev B*. 54 (1996) 9746–9755. doi:10.1103/PhysRevB.54.9746.
- [9] V.V. Khovailo, T. Takagi, A.N. Vasil'ev, H. Miki, M. Matsumoto, R. Kainuma, On Order-Disorder (L2<sub>1</sub>->B2') Phase Transition in Ni<sub>2+x</sub>Mn<sub>1-x</sub>Ga Heusler Alloys, *Phys Stat Sol.* 183 (2001) R1–R3. doi:10.1002/1521-396X(200102)183:2<R1::AID-PSSA99991>3.0.CO;2-B.
- [10] H. Yan, Y. Zhang, N. Xu, A. Senyshyn, H.G. Brokmeier, C. Esling, X. Zhao, L. Zuo, Liang Zuo, L. Zuo, Crystal structure determination of incommensurate modulated martensite in Ni-Mn-In Heusler alloys, *Acta Mater.* 88 (2015) 375–388. doi:10.1016/j.actamat.2015.01.025.
- [11] T. Krenke, M. Acet, E.F. Wassermann, X. Moya, L. Mañosa, A. Planes, Ferromagnetism in the austenitic and martensitic states of Ni-Mn-In alloys, *Phys Rev B*. 73 (2006) 174413. doi:10.1103/PhysRevB.73.174413.
- [12] C. Zhang, Y. Zhang, C. Esling, X. Zhao, L. Zuo, Crystallographic features of the martensitic transformation and their impact on variant organization in the intermetallic compound Ni<sub>50</sub>Mn<sub>38</sub>Sb<sub>12</sub> studied by SEM/EBSD, *IUCrJ*. 4 (2017) 700–709. doi:10.1107/S2052252517011332.
- [13] A. Planes, L. Mañosa, M. Acet, Magnetocaloric effect and its relation to shape-memory properties in ferromagnetic Heusler alloys, *J Phys Condens Matter*. 21 (2009) 223201. doi:10.1088/0953-8984/21/23/233201.
- [14] T. Krenke, E. Duman, M. Acet, E.F. Wassermann, X. Moya, L. Mañosa, A. Planes, Inverse magnetocaloric

- effect in ferromagnetic Ni-Mn-Sn alloys, *Nat Mater.* 4 (2005) 450–454. doi:10.1038/nmat1395.
- [15] K. Oikawa, W. Ito, Y. Imano, Y. Sutou, R. Kainuma, K. Ishida, S. Okamoto, O. Kitakami, T. Kanomata, Effect of magnetic field on martensitic transition of  $\text{Ni}_{46}\text{Mn}_{41}\text{In}_{13}$  Heusler alloy, *Appl. Phys. Lett.* 88 (2006) 122507. doi:10.1063/1.2187414.
- [16] C.M. Li, H.-B. Luo, Q.-M. Hu, R. Yang, B. Johansson, L. Vitos, Role of magnetic and atomic ordering in the martensitic transformation of Ni-Mn-In from a first-principles study, *Phys Rev B.* 86 (2012) 214205. doi:10.1103/PhysRevB.86.214205.
- [17] V.D. Buchelnikov, P. Entel, S. V. Taskaev, V. V. Sokolovskiy, A. Hucht, M. Ogura, H. Akai, M.E. Gruner, S.K. Nayak, Monte Carlo study of the influence of antiferromagnetic exchange interactions on the phase transitions of ferromagnetic Ni-Mn-X alloys (X=In, Sn, Sb), *Phys Rev B.* 78 (2008) 184427. doi:10.1103/PhysRevB.78.184427.
- [18] R.Y. Umetsu, A. Fujita, W. Ito, T. Kanomata, R. Kainuma, Determination of the magnetic ground state in the martensite phase of Ni-Mn-Z (Z = In, Sn and Sb) off-stoichiometric Heusler alloys by nonlinear AC susceptibility, *J Phys Condens Matter.* 23 (2011) 326001. doi:10.1088/0953-8984/23/32/326001.
- [19] K.R. Priolkar, P.A. Bhoje, D.N. Lobo, S.W. D'Souza, S.R. Barman, A. Chakrabarti, S. Emura, Antiferromagnetic exchange interactions in the  $\text{Ni}_2\text{Mn}_{1.4}\text{In}_{0.6}$  ferromagnetic Heusler alloy, *Phys Rev B.* 87 (2013) 144412. doi:10.1103/PhysRevB.87.144412.
- [20] K.R. Priolkar, D.N. Lobo, P.A. Bhoje, S. Emura, A.K. Nigam, Role of Ni-Mn hybridization in the magnetism of the martensitic state of Ni-Mn-In shape memory alloys, *EPL.* 94 (2011) 38006. doi:10.1209/0295-5075/94/38006.
- [21] R.Y. Umetsu, Y. Kusakari, T. Kanomata, K. Suga, Y. Sawai, K. Kindo, K. Oikawa, R. Kainuma, K. Ishida, Metamagnetic behaviour under high magnetic fields in  $\text{Ni}_{50}\text{Mn}_{50-x}\text{In}_x$  (x = 14.0 and 15.6) shape memory alloys, *J Phys D Appl Phys.* 42 (2009) 075003. doi:10.1088/0022-3727/42/7/075003.
- [22] T. Kanomata, T. Yasuda, S. Sasaki, H. Nishihara, R. Kainuma, W. Ito, K. Oikawa, K. Ishida, K. Neumann, K.R.A. Ziebeck, Magnetic properties on shape memory alloys  $\text{Ni}_2\text{Mn}_{1+x}\text{In}_{1-x}$ , *J Magn Magn Mater.* 321 (2009) 773–776. doi:10.1016/j.jmmm.2008.11.079.
- [23] E. Şaşıoğlu, L.M. Sandratskii, P. Bruno, First-principles calculation of the intersublattice exchange interactions and Curie temperatures of the full Heusler alloys  $\text{Ni}_2\text{MnX}$  (X = Ga, In, Sn, Sb), *Phys Rev B.* 70 (2004) 024427.

doi:10.1103/PhysRevB.70.024427.

- [24] E. Şaşıoğlu, L.M. Sandratskii, P. Bruno, Role of conduction electrons in mediating exchange interactions in Mn-based Heusler alloys, *Phys Rev B*. 77 (2008) 064417. doi:10.1103/PhysRevB.77.064417.
- [25] G. Kresse, J. Furthmüller, Efficient iterative schemes for ab initio total-energy calculations using a plane-wave basis set, *Phys Rev B*. 54 (1996) 11169–11186. doi:10.1103/PhysRevB.54.11169.
- [26] P. Cao, F. Tian, Y. Wang, Effect of Mo on the phase stability and elastic mechanical properties of Ti-Mo random alloys from ab initio calculations, *J Phys Condens Matter*. 29 (2017) 435703. doi:10.1088/1361-648X/aa87d3.
- [27] F. Tian, Y. Wang, L. Vitos, Impact of aluminum doping on the thermo-physical properties of refractory medium-entropy alloys, *J Appl Phys*. 121 (2017) 015105. doi:10.1063/1.4973489.
- [28] C.M. Li, Q.M. Hu, R. Yang, B. Johansson, L. Vitos, Understanding the martensitic phase transition of  $\text{Ni}_2(\text{Mn}_{1-x}\text{Fe}_x)\text{Ga}$  magnetic shape-memory alloys from theoretical calculations, *Phys Rev B*. 91 (2015) 174112. doi:10.1103/PhysRevB.91.174112.
- [29] J.P. Perdew, K. Burke, M. Ernzerhof, Generalized gradient approximation made simple, *Phys Rev Lett*. 77 (1996) 3865–3868. doi:10.1103/PhysRevLett.77.3865.
- [30] A. Ayuela, J. Enkoraara, K. Ullakko, R. M. Nieminen, Structural properties of magnetic Heusler alloys, *J Phys Condens Matter*. 11 (1999) 2017–2026. doi:10.1088/0953-8984/11/8/014.
- [31] V. V Godlevsky, K.M. Rabe, Soft tetragonal distortions in ferromagnetic  $\text{Ni}_2\text{MnGa}$  and related materials from first principles, *Phys Rev B*. 63 (2001) 134407. doi:10.1103/PhysRevB.63.134407.
- [32] D.Y. Cong, P. Zetterström, Y.D. Wang, R. Delaplane, R.L. Peng, X. Zhao, L. Zuo, Crystal structure and phase transformation in  $\text{Ni}_{53}\text{Mn}_{25}\text{Ga}_{22}$  shape memory alloy from 20K to 473K, *Appl Phys Lett*. 87 (2005) 111906. doi:10.1063/1.2043250.
- [33] Z. Li, Y. Jiang, Z. Li, C.F.S. Valdés, José Luis Sánchez Llamazares, B. Yang, Y. Zhang, C. Esling, X. Zhao, L. Zuo, Phase transition and magnetocaloric properties of  $\text{Mn}_{50}\text{Ni}_{42-x}\text{Co}_x\text{Sn}_8$  ( $0 \leq x \leq 10$ ) melt-spun ribbons, *IUCrJ*. 5 (2018) 54–66. doi:10.1107/S2052252517016220.
- [34] A.K. Pathak, M. Khan, I. Dubenko, S. Stadler, N. Ali, Large magnetic entropy change in  $\text{Ni}_{50}\text{Mn}_{50-x}\text{In}_x$  Heusler alloys, *Appl Phys Lett*. 90 (2007) 262504. doi:10.1063/1.2752720.
- [35] L. Vitos, Computational quantum mechanics for materials engineers: the EMTO method and applications,

Springer US, Boston, MA, 2005. doi:10.1007/978-1-84628-951-4.

- [36] David Sholl, J.A. Steckel, Density functional theory: a practical introduction, New Jersey, Canada, 1999.  
doi:10.1002/9780470447710.